Inorganic Chemistry

Article

pubs.acs.org/IC

Crystallographic and Computational Studies of Luminescent, Binuclear Gold(I) Complexes, $Au^{I}_2(Ph_2P(CH_2)_nPPh_2)_2I_2$ (n = 3−6)

Sang Ho Lim,[†] Jennifer C. Schmitt,[‡] Jason Shearer,*[,‡] Jianhua Jia,[†] Marilyn M. Olmstead,[†] James C. Fettinger,[†] and Alan L. Balch*[,†]

[†]Department of Chemistry, University of California, Davis, California 95616, United States

[‡]Department of Chemistry, University of Nevada, Reno, Nevada 89557, United States

Supporting Information

ABSTRACT: Four crystalline dimers of the type, $Au^{I}_2(\mu\text{-}PnP)_2I_2$, where PnP is $PPh_2(CH_2)_nPPh_2$ with n = 3, 4, 5, and 6 have been prepared and characterized by single-crystal X-ray diffraction and by ^{31}P NMR and infrared spectroscopy. $Au^{I}_2(\mu\text{-}P3P)_2I_2$ and $Au^{I}_2(\mu\text{-}P6P)_2I_2$ are centrosymmetric dimers with the planar $Au^{I}P_2I$ units oriented in antiparallel fashion. Remarkably, noncentrosymmetric $Au^{I}_2(\mu\text{-}P5P)_2I_2$ has its planar $Au^{I}P_2I$ units oriented in parallel manner. $Au^{I}_2(\mu\text{-}P4P)_2(\mu\text{-}I)_2$ is unique, since it contains four-coordinate gold centers that are bridged by both iodide and diphosphine ligands. All four compounds are luminescent as solids at room temperature. B3LYP, B2PLYP, and spectroscopically oriented configuration interaction (SORCI) calculations have been conducted to give insight into the electronic and geometric structures of the ground and first excited triplet states of the three trigonal-planar complexes. The emission energies for the trigonal planar complexes are more strongly correlated with changes in the Au−I bond length rather than changes in the P−Au−P angle.

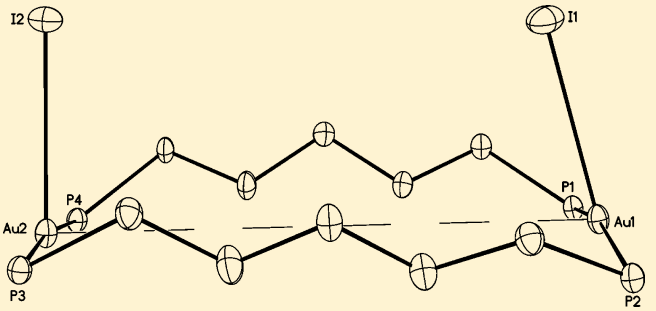

INTRODUCTION

The luminescence arising from gold(I) complexes has received considerable attention.[1−4] While monomeric, two-coordinate gold(I) complexes are generally nonemissive, they can become emissive when aurophilic interactions between gold(I) centers are allowed to occur. Such aurophilic interactions are attractive connections between gold centers that are promoted by a combination of relativistic and correlation effects.[5−8] Although many two-coordinate gold(I) complexes are nonluminescent in solution, they can become luminescent in the solid state because of self-association through aurophilic interactions.[9−11]

Mononuclear three-coordinate gold(I) complexes with a planar geometry are frequently luminescent both in the solid state and in solution.[12−14] In general, aurophilic interactions are not needed for three-coordinate gold(I) complexes to be emissive.

Recently, the remarkably flexible molecule, $Au_2(\mu\text{-dppe})_2Br_2$, was shown to be a trigonal-planar complex in which aurophilic interactions influenced the luminescence.[15] Dimeric $Au_2(\mu\text{-dppe})_2Br_2$ can accommodate Au···Au separations that range from 3.8479(3) to 3.0995(10) Å. These different Au···Au separations occur in an array of crystalline solvates of the dimer. Variations in the Au···Au separations along with alterations in the Au−Br distances and in the P−Au−P angles result in differences in the luminescence properties of crystals of $Au_2(\mu\text{-dppe})_2Br_2$. Crystals with Au···Au separations less than 3.5 Å show green luminescence, while those with Au···Au separations greater than 3.5 Å display orange luminescence. Additionally, we have reported the solid state interconversions of four different crystalline compounds containing the $Au_2(dppe)_2I_2$ unit (dppe is bis-(diphenylphosphino)ethane) that have been observed and characterized through X-ray diffraction and emission spectroscopy.[16]

For monomeric, trigonal planar complexes that lack aurophilic interactions, the excitation process is generally attributed to a transition from the filled, in-plane $d_{x^2-y^2}$,d_{xy} orbitals on gold into a suitable empty orbital, which may be the gold p_z orbital or a ligand-based orbital. Several experimental and computational studies have examined the structural changes that are involved during excitation of three-coordinate gold(I) complexes. For complexes of the types $[Au(PR_3)_3]^+$ and $Au(PR_3)_2X$ (X = halide) excitation is proposed to cause extensive distortion from a trigonal planar ground state to a distorted T-shape or beyond for the lowest triplet excited state.[17,18] Photocrystallographic studies of $Au(PR_3)_2Cl{\cdot}CHCl_3$ and $Au(PR_3)_2Cl$ showed bond shortening in the excited state.[19,20] However, a similar study of a second polymorph of $Au(PR_3)_2Cl$ revealed little change between the structures of the crystals before and after photoexcitation.[21]

Here we report on the preparation, structure, and luminescence of a series of trigonal planar gold(I) complexes that were designed under the naïve notion that chelated monomers shown in Scheme 1 could be prepared from the

Received: September 6, 2012

   dx.doi.org/10.1021/ic301954n | Inorg. Chem. XXXX, XXX, XXX−XXX

Scheme 1. Trigonal Planar Au^I Compounds

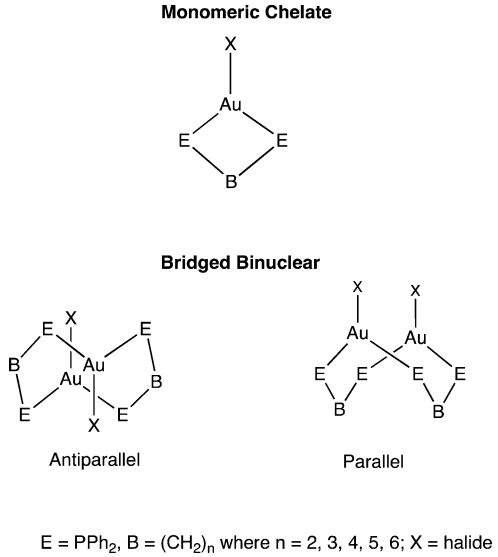

diphosphine ligands, $Ph_2P(CH_2)_nPPh_2$, and that alteration of the length of the polymethylene chain would alter the P−Au−P angles in these complexes in a sensible fashion. As shown below, such chelated monomers were not obtained. Rather bridged, binuclear complexes were obtained.

RESULTS AND DISCUSSION

Synthesis and Crystal Growth. The reaction of a suspension of Au^II with the appropriate P*n*P ligand (n = 3−6) produces colorless solids that can be crystallized from dichloromethane/diethyl ether or chloroform/diethyl ether to yield colorless crystals of the dimeric products. Infrared and ^{31}P NMR spectra of these compounds are given in the Experimental Section. The ^{31}P NMR spectra for all four complexes consist of a single resonance and indicate that all phosphorus atoms in the complexes are equivalent.

Structure of $Au^I_2(\mu$-P3P$)_2I_2$. Crystal data for all complexes considered here are given in Table 1. Selected bond distances and angles are presented in Tables 2 and 3. For comparison, structural data for the monomeric $Au^I(PPh_3)_2I$ is included in the tables.[22] A drawing of the structure of $Au^I_2(\mu$-P3P$)_2I_2$ is shown in Figure 1. The dimeric $Au^I_2(\mu$-P3P$)_2I_2$ molecule packs about a crystallographic center of symmetry so that one-half of the dimer resides in the asymmetric unit. The gold center is three-coordinate with bonds to two phosphorus atoms of two different bridging ligands and to the terminal iodide ligand. The Au^IP_2I unit is planar. The sum of the two P−Au−I angles and the P−Au−P angle is 359.8°, but these individual bond angles themselves differ considerably. The centrosymmetric nature of the complex positions the two polar Au^IP_2I units in an antiparallel alignment. The Au···Au separation is rather long, 5.0671(6) Å, and there is no significant aurophilic interaction within the molecule.

Figure 2 shows a drawing of just the 12-membered ring of atoms at the center of $Au^I_2(\mu$-P3P$)_2I_2$. This view emphasizes the antiparallel orientation of the two Au^IP_2I planes. Figure 2 also shows a comparable view of the other three compounds reported here.

Structure of $Au^I_2(\mu$-P4P$)_2(\mu$-I$)_2$. A drawing of a molecule of $Au^I_2(\mu$-P4P$)_2(\mu$-I$)_2$ is shown in Figure 3. One half of the molecule is present in the asymmetric unit. The rest of the molecule is generated by inversion through the crystallographic center of symmetry. Within the series of four molecules considered here, $Au^I_2(\mu$-P4P$)_2(\mu$-I$)_2$ is the only one with four-coordinate gold ions. The gold ion is in a highly distorted tetrahedral environment with bonds to two phosphorus atoms and two bridging iodide ligands. The two Au−I distances (3.0580(3), 3.0967(4) Å) are nearly equal. These are the longest Au−I bonds seen in this series of molecules. Likewise, the two Au−P distances (2.3092(7), 2.3248(6) Å) are nearly

Table 1. Crystal Data and Structure Refinement for $Au^I_2(\mu$-P*n*P$)_2I_2$

	$Au^I_2(\mu$-P3P$)_2I_2$	$Au^I_2(\mu$-P4P$)_2(\mu$-I$)_2$	$Au^I_2(\mu$-P5P$)_2I_2\cdot3CHCl_3$	$Au^I_2(\mu$-P6P$)_2I_2$
formula	$C_{54}H_{52}Au_2I_2P_4$	$C_{56}H_{56}Au_2I_2P_4$	$C_{58}H_{60}Au_2I_2P_4\cdot3(CHCl_3)$	$C_{60}H_{64}Au_2\ I_2P_4$
formula weight	1472.58	1500.62	1885.77	1556.73
T, K	90(2)	90(2)	90(2)	90(2)
color and habit	colorless block	colorless block	colorless block	colorless block
crystal system	triclinic	monoclinic	monoclinic	triclinic
space group	$P\bar{1}$	$P2_1/c$	$P2_1$	$P\bar{1}$
a, Å	10.527(5)	10.124(2)	10.821(2)	9.984(2)
b, Å	10.853(5)	18.692(2)	20.111(4)	11.648(2)
c, Å	12.979(5)	15.574(2)	15.845(3)	12.673(2)
α, deg	91.340(5)	90	90	101.425(5)
β, deg	113.602(5)	119.930(5)	94.334(1)	93.982(5)
γ, deg	111.965(5)	90	90	100.789(5)
V, Å^3	1233.7(9)	2554.1(7)	3438.4(11)	1410.3(4)
Z	1	2	2	1
d_{calcd}, g cm^{-3}	1.982	1.951	1.821	1.833
μ, mm^{-1}	7.356	7.108	5.639	6.440
unique data	5673	7857	20323	6463
restraints	0	0	1	0
params.	145	289	701	307
R1[a]	0.0356	0.0189	0.0221	0.0140
wR2[b]	0.0758	0.0396	0.0559	0.0332

[a]For data with $I > 2\sigma I$, $R1 = \sum||F_o| - |F_c||/\sum|F_o|$. [b]For all data. $wR2 = [\sum w(F_o^2 - F_c^2)^2/\sum w(F_o^2)^2]^{1/2}$.

dx.doi.org/10.1021/ic301954n | Inorg. Chem. XXXX, XXX, XXX−XXX

Table 2. Selected Experimental and Computed Bond Distances (Å) for $Au^{I}_2(\mu\text{-P}n\text{P})_2I_2$ and $AuI(PPh_2R)I$

bond lengths, Å	$Au^{I}_2(\mu\text{-P3P})_2I_2$	$Au^{I}_2(\mu\text{-P4P})_2I_2$	$Au^{I}_2(\mu\text{-P5P})_2I_2\cdot 3CHCl_3$	$Au^{I}_2(\mu\text{-P6P})_2I_2$	$Au^{I}(PPh_2R)_2I$
Au1−I1	2.9310(14)[a]	3.0580(3)	3.0006(6)	2.8052(4)	2.754(1) Ph[d]
	{3.051}[b]		{3.007}	{2.973}v	{2.970} Me
	[3.115][c]		[3.079]	[2.953]	[2.906] Me
Au2−I2		3.0967(4)	3.0831(7)		
			{3.016}		
			[3.098]		
Au1−P1	2.3048(18)	2.3092(7)	2.3089(9)	2.3347(6)	2.333(2) Ph[d]
	{2.372}		{2.378}	{2.402}	{2.409} Me
	[2.383]		[2.354]	[2.385]	[2.662] Me
Au1−P2	2.3217(17)	2.3248(6)	2.3017(9)	2.2997(6)	
	{2.393}		{2.378}	{2.375}	{2.412} Me
	[2.390]		[2.365]	[2.384]	[2.665] Me
Au2−P3			2.3093(8)		
			{2.379}		
			[2.386]		
Au2−P4			2.3115(8)		
			{2.379}		
			[2.341]		
Au···Au	5.0671(6)	4.1952(2)	8.0206(3)	5.3095(2)	
	{5.151}		{8.089}	{5.595}	
	[5.247]		[8.242]	[7.011]	

[a]Experimental. [b]{} Computed for the Ground State. [c][] Computed for the First Excited Triplet. [d]Data from Bowmaker, G. A.; Dyason, J. C.; Healy, P. C.; Engelhardt, M.; Pakawatchai, C.; White, A. H. *J. Chem. Soc., Dalton Trans.* **1987**, 1089.

Table 3. Selected Experimental and Computed Bond Angles (deg) for $Au^{I}_2(\mu\text{-P}n\text{P})_2I_2$ and $AuI(PPh_2R)_2I$

bond angles (deg)	$Au^{I}_2(\mu\text{-P3P})_2I_2$	$Au^{I}_2(\mu\text{-P4P})_2(\mu\text{-I})_2$	$Au^{I}_2(\mu\text{-P5P})_2I_2\cdot 3CHCl_3$	$Au^{I}_2(\mu\text{-P6P})_2I_2$	$Au^{I}(PPh_2R)_2I$
P1−Au1−P2	152.88(5)[a]	143.31(2)	164.63(3)	133.042(19)	132.13(7) Ph[d]
	{155.0}[b]		{164.0}	{136.1}	{147.3} Me
	[163.3][c]		[175.3]	[158.3]	[179.8] Me
P3−Au2−P4			172.32(3)		
			{164.9}		
			[170.6]		
P1−Au1−I1	109.14(4)	96.218(15)	94.19(2)	102.311(19)	113.93(5) Ph[d]
	{108.9}		{96.7}	{115.7}	{107.1} Me
	[103.3]		[90.2]	[106.8]	[90.0] Me
P1−Au1−I1A		105.098(15)			
P2−Au1−I1	97.77(4)	115.841(16)	101.01(2)	123.086(15)	
	{96.0}		{98.2}	{102.1}	{105.4} Me
	[93.4]		[88.7]	[94.5]	[90.5] Me
P2−Au1−I1A		92.369(19)			
P3−Au2−I2			93.45(2)		
			{98.5}		
			[95.3]		
P4−Au2−I2			93.36(2)		
			{97.2}		
			[94.0]		
I1−Au1−I1A		94.061(10)			

[a]Experimental. [b]{} Computed for the Ground State. [c][] Computed for the First Excited Triplet. [d]Data from Bowmaker, G. A.; Dyason, J. C.; Healy, P. C.; Engelhardt, M.; Pakawatchai, C.; White, A. H. *J. Chem. Soc., Dalton Trans.* **1987**, 1089.

equivalent and are similar to those of the other molecules reported here. As best seen in Figure 2, the iodide ligands lie well outside of the planes of the two P−Au−P units.

Structure of $Au^{I}_2(\mu\text{-P5P})_2I_2$. The structure of $Au^{I}_2(\mu\text{-P5P})_2I_2$ is shown in Figure 4. This is the only noncentrosymmetric molecule in the series reported here. It has no crystallographically imposed symmetry, and there are some significant differences in the bond lengths and angles involving the two gold centers. Each gold ion has planar, three-coordinate geometry. For Au1, the sum of the two P−Au−I angles and the P−Au−P angle is 359.83°, while for Au2 that sum is 359.13°. Notice that the P−Au−P angles (164.63(3), 172.32(3)°) are quite wide. Remarkably, the two polar $Au^{I}P_2I$ units are aligned in parallel fashion as can be seen in Figures 2 and 4.

Structure of $Au^{I}_2(\mu\text{-P6P})_2I_2$. Figure 5 shows a drawing of the $Au^{I}_2(\mu\text{-P6P})_2I_2$ molecule. The molecule resides at a crystallographic center of symmetry with one-half of the molecule in the asymmetric unit. The structure of $Au^{I}_2(\mu$-

dx.doi.org/10.1021/ic301954n | *Inorg. Chem.* XXXX, XXX, XXX−XXX

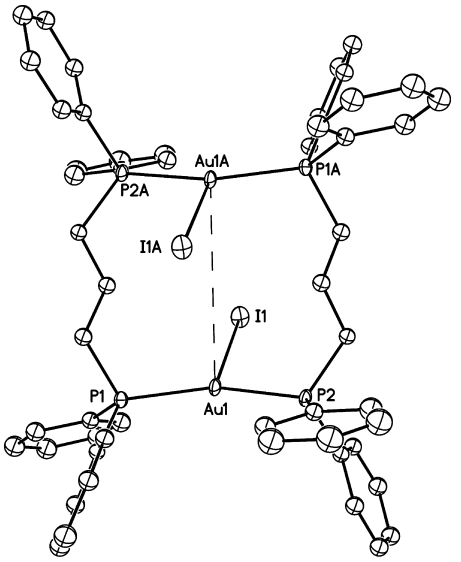

Figure 1. Drawing of the structure of $Au^{I}_{2}(\mu\text{-P3P})_2I_2$. Thermal ellipsoids are shown at the 50% probability level. Hydrogen atoms are not shown for clarity.

P6P)$_2$I$_2$ is similar to that of $Au^{I}_{2}(\mu\text{-P3P})_2I_2$ with the two planar $Au^{I}P_2I$ units arranged in antiparallel fashion as is apparent in the perspective used in Figure 2. The sum of the two P−Au−I angles and the P−Au−P angle is 358.44°.

Luminescence. Each of the compounds is luminescent at room temperature. Figure 6 shows the emission and excitation spectra for the planar, three-coordinate complexes, $Au^{I}_{2}(\mu\text{-P3P})_2I_2$, $Au^{I}_{2}(\mu\text{-P5P})_2I_2$, and $Au^{I}_{2}(\mu\text{-P6P})_2I_2$. The excitation profiles for these three complexes are similar, but the emission maxima differ. The absorption maxima increase as the length of the methylene chain (and hence n) increases, but there is no apparent correlation of the emission energies with the P−Au−P angles in the ground state of these molecules. Four-coordinate $Au^{I}_{2}(\mu\text{-P4P})_2(\mu\text{-I})_2$ is also luminescent with an excitation maximum at 353 nm and emission maximum at 440 nm.

Optimized Geometric Structures from Computational Studies. To better understand the connection between the structure of these complexes and their corresponding luminescence properties, electronic structure calculations of these complexes were performed. To obtain input structures for these compounds, geometry optimizations (GOs) were performed using the widely employed B3LYP hybrid density functional on the compounds $Au^{I}_{2}(\mu\text{-P3P})_2I_2$ (n3), $Au^{I}_{2}(\mu\text{-P5P})_2I_2$ (n5), and $Au^{I}_{2}(\mu\text{-P6P})_2I_2$ (n6). To determine the influence of the tether on the $Au^{I}P_2I$ unit, we also performed a GO at the B3LYP level on the unconstrained compound $Au^{I}(PPh_2Me)_2I$. These calculations utilized a large def2-TZVPP basis set[23] for all atoms except gold, which was treated with a VTZ-PP basis set on the valence electrons[24] and the Stuttgart/Bonn pseudopotential (ECO60MDF) on all core electrons.[25] The resulting singlet state GO structures of n3 and n6 are in good agreement with the experimental data (Tables 2 and 3). We note that there is a small but consistent overestimation of the Au-ligand bond lengths in the B3LYP structures vs the experimentally determined bond lengths; however, this is a well-known artifact of the B3LYP functional.[26]

For n5 the computations produced the unusual parallel alignment of the two AuP_2I units seen in Figures 2 and 4, but the large differences in the two gold(I) centers observed

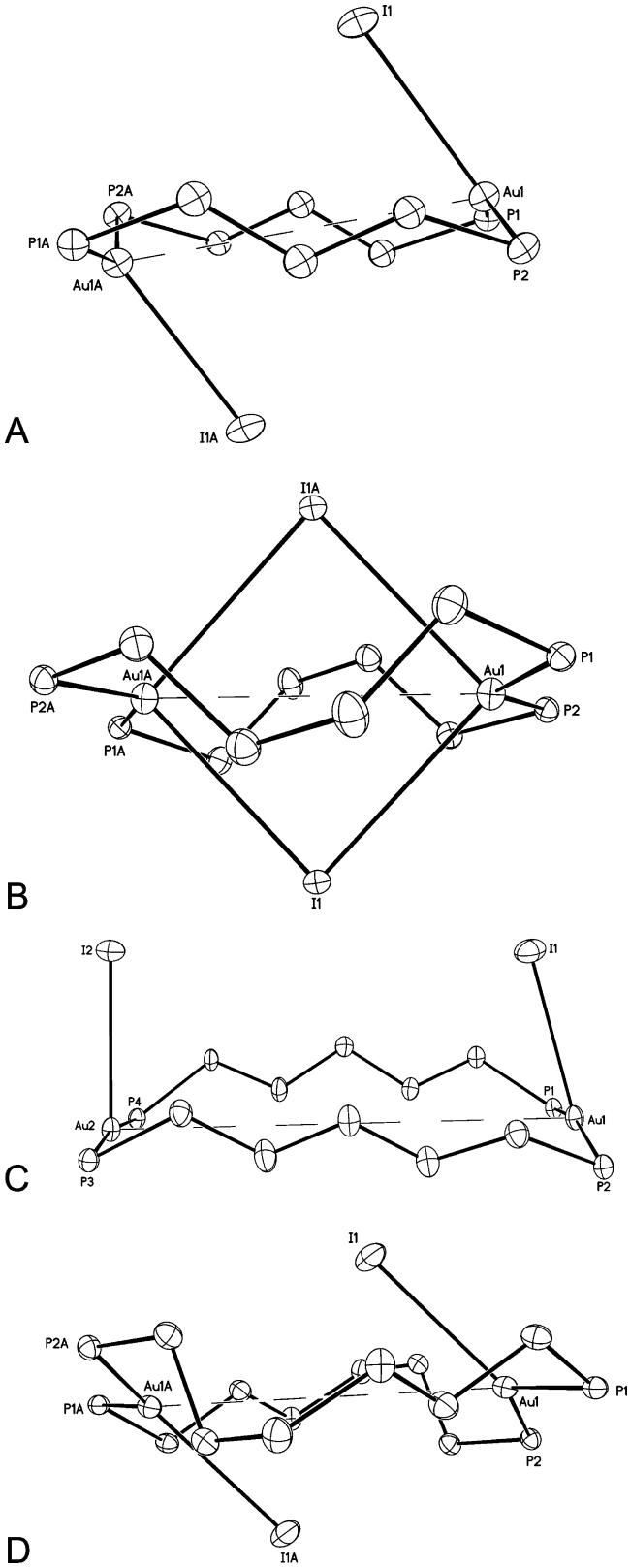

Figure 2. Comparison of the ring conformations of $Au^{I}_{2}(\mu\text{-P}n\text{P})_2I_2$; (A) n = 3, (B) n = 4, (C) n = 5, (d) n = 6. For reference, the dashed lines connect the gold centers.

experimentally could not be reproduced; we find that both gold(I) centers in the GO structure of n5 are similar to one another. Although some asymmetry is observed between the

dx.doi.org/10.1021/ic301954n | Inorg. Chem. XXXX, XXX, XXX−XXX

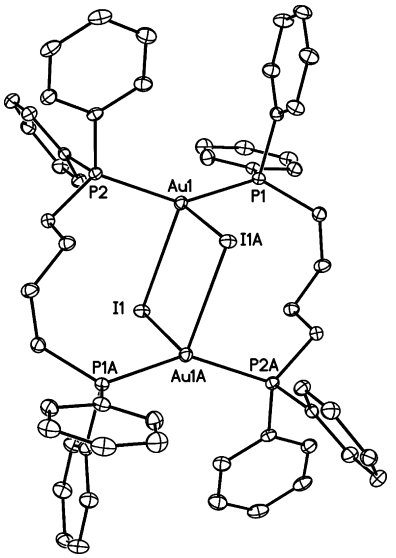

Figure 3. Drawing of the structure of $Au^{I}_{2}(\mu\text{-P4P})_2(\mu\text{-I})_2$. Thermal ellipsoids are shown at the 50% probability level. Hydrogen atoms are not shown for clarity.

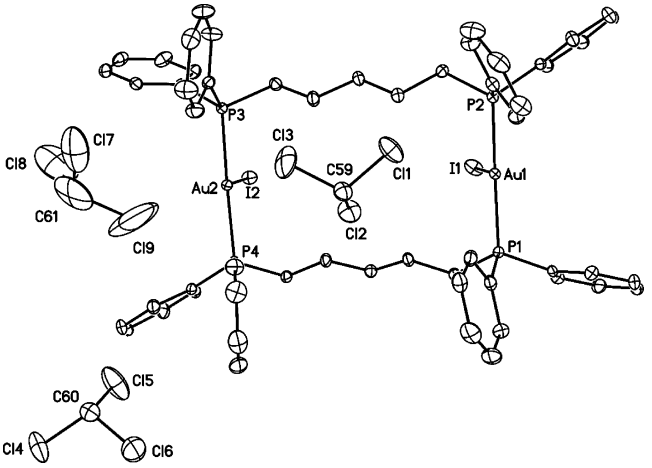

Figure 4. Drawing of the structure of $Au^{I}_{2}(\mu\text{-P5P})_2I_2\cdot 3CHCl_3$. Thermal ellipsoids are shown at the 50% probability level. Hydrogen atoms are not shown for clarity.

two gold(I) centers, the difference between the two gold(I) geometries is minor (Tables 2 and 3). The two Au-centers in the GO structure of n5 are most consistent with the less open P−Au−P bond angle of $Au^{I}_{2}(\mu\text{-P5P})_2I_2$ (labeled Au2) derived crystallographically. Even at the MP2 level of theory the asymmetry observed for the two gold(I)-centers in $Au^{I}_{2}(\mu\text{-P5P})_2I_2$ cannot be reproduced; we observe that the two P−Au−P bond angles remain at ∼165°.

There are two key metric parameters of note in the discussion below: the P−Au−P bond angles and the Au−I bond lengths (Tables 2 and 3). The calculated P−Au−P bond angles increase from 136.1° (n6) to 155.0° (n3) to 164.1° (n5), as is observed crystallographically. Compound n6 possesses metric parameters that are the closest to $Au^{I}(PPh_2Me)_2I$, but it still demonstrates significant distortions from the untethered compound. Thus, all of the tethered complexes demonstrate significant asymmetry from the unconstrained compound $Au^{I}(PPh_2Me)_2I$. These differences in metric parameters between the complexes are likely a result of the polymethylene

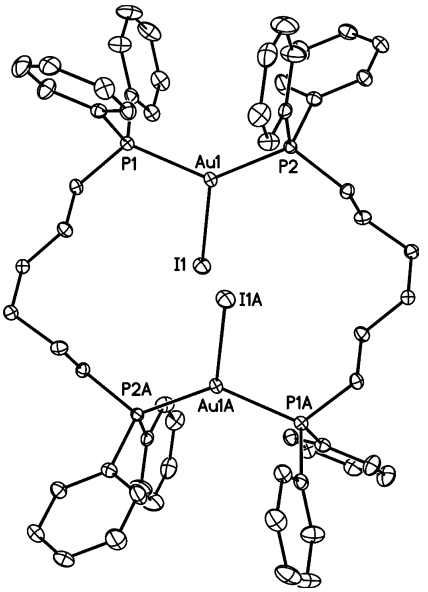

Figure 5. Drawing of the structure of $Au^{I}_{2}(\mu\text{-P6P})_2I_2$. Thermal ellipsoids are shown at the 50% probability level. Hydrogen atoms are not shown for clarity.

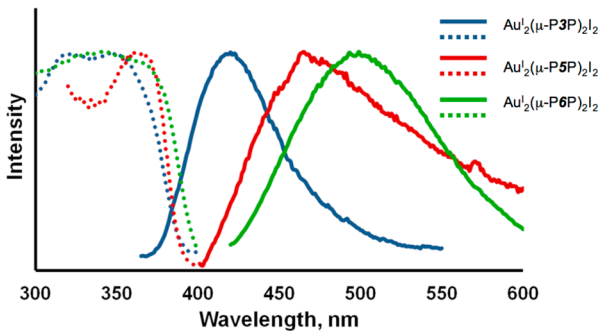

Figure 6. Emission spectra for crystals of the planar, three-coordinate complexes $Au^{I}_{2}(\mu\text{-P}n\text{P})_2I_2$ (n = 3, 5, 6) at room temperature.

tether, which is undoubtedly influencing the geometry about the gold(I) center.

Unlike the P−Au−P bond angles, the Au−I bond lengths display a systematic trend across the n3−n6 series. As the polymethylene tether increases there is a systematic decrease in the Au−I bond length; the bond-length decreases from 3.051 Å (n3) to 2.973 Å (n6). At 2.970 Å, the unconstrained compound $Au^{I}(PPh_2Me)_2I$ demonstrates the shortest Au−I bond length of the compounds examined computationally. The elongation of the Au−I bond length as the polymethylene tether is shortened can be readily rationalized. There are significant steric interactions between the I atom and the methylene H atoms. As the tether is elongated the phenyl groups are more capable of "splaying open" allowing the methylene groups to open up away from the Au−Au central axis. Thus, the Au−I bond length can contract.

In addition to the ground state singlet structure (S0), we also performed GOs of the first triplet excited state (T1) of n3, n5, n6, and $Au^{I}(PPh_2Me)_2I$. Selected metric parameters are shown in Tables 2 and 3. The untethered complex $Au^{I}(PPh_2Me)_2I$ displays an excited state geometry with all of the hallmarks of those reported for other three coordinate gold(I) complexes in their first excited triplet state.[16,17] The overall structure is best described as T-shaped; the P−Au−I bond angle compresses to

dx.doi.org/10.1021/ic301954n | Inorg. Chem. XXXX, XXX, XXX−XXX

~90° and the P−Au−P opens to 179.8°. The Au−P bond length increases by ~0.3 Å to 2.66 Å, while the Au−I bond length undergoes a contraction to 2.91 Å. In contrast, the T1 surface for n3, n5, and n6 are not T-shaped. Furthermore, the same nonsystematic changes in the P−Au−P bond angle observed on the S0 surface are reflected on the T1 surface. The P−Au−P bond angles become progressively more open from n6 (158.3°) to n3 (163.3°) to n5 (170.6/175.3°). Thus, the polymethylene tether is imposing significant geometric constraints on the T1 surface as well as the S0 surface.

Calculated Excitation and Emission Energies. Using the GO structures from above we calculated the energies of the S1 ← S0 and T1 → S0 transition energies. To achieve a high degree of accuracy for these excitation and emission energies we employed Neese's spectroscopically oriented configuration interaction (SORCI) methodology.[27] Unlike time-dependent density functional theory (TD-DFT) methods, the SORCI method is a true multiconfigurational, ab initio computational technique, and thus yields far more accurate excited state energies.[28] For these SORCI calculations, a modest CAS(4,4) reference space was utilized, which proved adequate to reproduce the experimentally observed excitation and emission energies (Table 4). The S1 ← S0 excitation energies for n3, n5, n6, and $Au^{I}(PPh_2Me)_2I$ are all similar to one another, and similar to those experimentally observed. In all cases we see the lowest energy excitation corresponds to a wavelength of ~390 nm. Thus, the calculations strongly suggest that the nature of the initial excitation process is best described as an excitation from the first to second singlet surfaces. In all of these cases the excitation process is best described as a metal-to-ligand charge-transfer (MLCT) process originating from a state composed of mostly $Au(5d_{xy})/I(5p_x)$ antibonding character to a state that is composed of exclusively phosphine ligand character (Figure 7a).

Table 4. Computed and Experimental Excitation and Emission Maxima for Trigonal Planar Gold(I) Complexes

compd		n3	n5	n6	$Au^{I}IP_2$
S1 ← S0 (nm) excitation	computed	387	388	391	390
	experimental	370 sh	370	380	
T1 → S0 (nm) emission	computed	425	486	505	529
	experimental	420	465	499	

The lowest energy T1 → S0 emission process corresponds to roughly the inverse of the excitation process; it corresponds to a decay from a state corresponding to phosphine-ligand character to a state composed of $Au(5d_{xy})/I(5p_x)$ antibonding character (Figure 7b). Despite the fact that the lowest energy emissions are all T1 → S0 processes originating from similar states, we calculate different emission energies for all four compounds investigated. There is a systematic red-shift in emission energies as the polymethylene tether is elongated. Compound n3 has a calculated emission energy of 425 nm, n5 has an emission energy of 476 nm, while n6 has its emission maximum at 505 nm. Untethered $Au^{I}(PPh_2Me)_2I$ displayed the most red-shifted emission energy of all of the compounds investigated (529 nm).

Origin of the Differential Emission Energies. Of the different structural parameters, the two parameters that vary the most from the S0 to the T1 structures are the Au−I bond length and the P−Au−P bond angle. The potential energy surfaces (PESs) of $Au^{I}(PPh_2Me)_2I$ were, therefore, constructed for the lowest energy singlet and triplet surfaces to examine the influence of the P−Au−P bond angle distortion and the Au−I bond length. Geometries for the PESs were constructed at the B3LYP level of theory using $Au^{I}(PPh_2Me)_2I$. To deconvolve the influence of the P−Au−P bond angle on the Au−I bond length and the Au−I bond length on the P−Au−P bond angle constrained GOs were performed. The PESs examining the P−Au−P bond distortion (from 105 to 180° in 2.5° increments) utilized a constrained Au−I bond length of 3.000 Å, while the PESs examining the Au−I bond length (from 2.800 to 3.150 Å in 0.025 Å increments) utilized a P−Au−P bond angle of 160°. Final single-point energies for each GO structure along the S0 and T1 surfaces were calculated using the B2PLYP double-hybrid functional.[29] This functional is similar to the B3LYP hybrid-functional, except it also mixes in a second-order Møller−Plesset perturbation theory (MP2) correction (along with the Hartee−Fock (HF) correction) to the DFT derived energies yielding highly accurate energies.[29,30]

The PES for the S0 state results in a rather shallow energy profile as the P−Au−P (Figure 8a). There is a minimum on the PES for $Au^{I}(PPh_2Me)_2I$ (Au−I bond length 3.000 Å) at 138.3°, which increase to 9.9 kJ mol^{-1} at 180°. There is another maximum observed at 105°, which at 9.4 kJ mol^{-1} is not as positive in energy as the point at 180°. This can be contrasted with the T1 surface, where the range of 132−136° represents a maximum on the T1 surface. In contrast there is a minimum of the T1 surface at 175.3°, which is 19.3 kJ mol^{-1} lower in energy than the maximum at 132.2°. This is consistent with the nature of the electronic structures of the two states. Along the T1 surface the highest occupied molecular orbital (HOMO) is made of a P(σ)-Au(6s) antibonding interaction. As the bond distorts from 180° to 132.2° more Au(6s) character becomes mixed into the HOMO, and the Au−P bonds become more

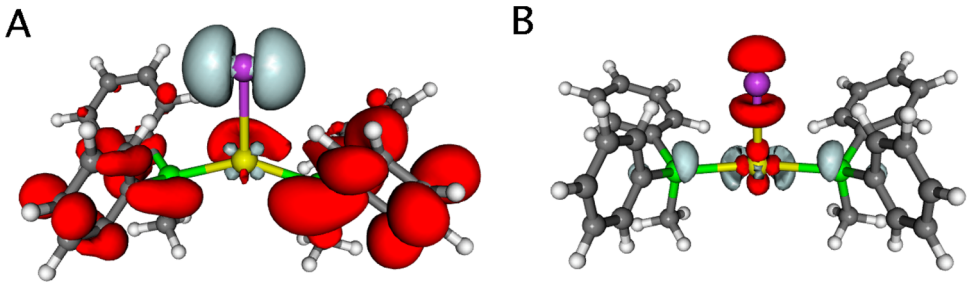

Figure 7. Isosurface transition difference plots derived from the SORCI calculations (TZVPP/VTZ-PP-ECP) for the (**A**) S1← S0 and (**B**) T1→ S0 transitions for $Au^{I}IP_2$. The red areas correspond to the regions of the molecule that are gaining electron density while the ice-blue areas correspond to regions of the molecule that are losing electron density.

dx.doi.org/10.1021/ic301954n | Inorg. Chem. XXXX, XXX, XXX−XXX

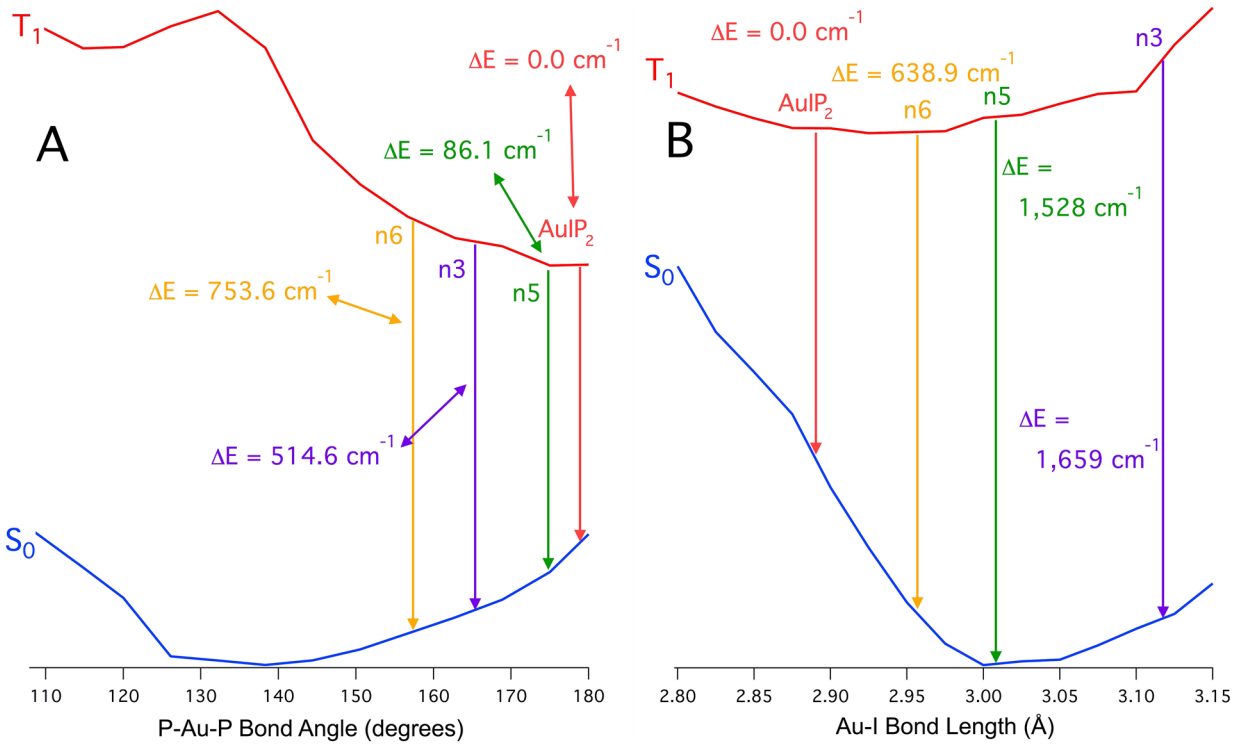

Figure 8. (**A**) B2PLYP (TZVPP/VTZ-PP-ECP) PES constructed for the P−A−P bond angle distortion maintaining a constant Au−I bond length. The vertical lines represent the transitions from the T1 to S0 surfaces based on the predicted excited state P−Au−P bond angles from the B3LYP geometry optimized structures. Energies are relative to the $Au^{I}P_2I$ T1 → S0 transition. (**B**) B2PLYP (TZVPP/VTZ-PP-ECP) PES constructed for Au−I bond length distortion with a fixed P−Au−P bond angle.

covalent. Thus, the antibonding HOMO of the T1 state increases in energy as the P−Au−P bond angle contracts, and the overall energy of the compound increases. In contrast, the P(σ)-Au(6s) covalency is not strongly affected along the S0 surface as the bond distorts, hence the rather small influence on the energy of the S0 state as the P−Au−P bond angle is distorted.

This can be contrasted with the changes in the energy of the S0 and T1 surfaces as the Au−I bond length is altered (Figure 8b). For the S0 state there is a large change in energy as the Au−I bond length changes. There is a minimum along the S0 PES for $Au^{I}(PPh_2Me)_2I$ at 2.982 Å (P−Au−P bond angle 160°). Contraction of the Au−I bond length to 2.800 Å leads to a 37.6 kJ mol^{-1} increase in energy, while elongation to 3.150 Å leads to only a 7.7 kJ mol^{-1} increase in energy. In contrast with the S0 surface, the T1 surface shows little influence in the change of energy as the Au−I bond length is altered. A contraction of the Au−I bond length from the equilibrium bond length of 2.911 Å on the T1 surface to 2.800 Å shows an increase in energy of only 3.8 kJ mol^{-1}, while elongation of the bond to 3.150 Å leads to an increase of 11.81 kJ mol^{-1}. Once again, we can relate this to the electronic structure of the S0 vs T1 states. The HOMO of the S0 state is composed of a Au($5d_{x2-y2}$)/I($5p_z$) antibonding interaction. As one compresses the Au−I bond, the Au−I bond covalency increases and the energy of the HOMO increases. Hence, the energy of the state increases. In contrast, contraction of the Au−I bond length leaves the T1 surface virtually unaltered; as we have relieved antibonding character in the Au−I bond, contraction of the Au−I bond is not as energetically unfavorable on the T1 PES.

Using the constructed PESs we can determine the emission energies of $Au^{I}(PPh_2Me)_2I$ as a function of P−Au−P bond angle and Au−I bond length. Along the P−Au−P PES we predict a small change in the T1 → S0 energy as the bond P−Au−P bond angle is closed, with a ΔE = 753.6 cm^{-1} going from the least energetic emission energy ($Au^{I}(PPh_2Me)_2I$) to the largest emission energy (n6). For the Au−I bond length PES we see a more dramatic change in emission energy as a function of Au−I bond length with a ΔE = 1,659 cm^{-1} going from $Au^{I}(PPh_2Me)_2I$ to n3.

Combining the energies of the two PESs allows us to understand the origins in the emission energies. Although the observed ΔE from the PESs are underestimated by at least one-half, the trend obtained in the SORCI calculations and the experimental data is observed. From the PES results we derive a systematic change in emission energies as the polymethylene tether length is increased. Compound n3 would be predicted to have the highest emission energy while $Au^{I}(PPh_2Me)_2I$ will have the lowest emission energy. This compares well with both the SORCI calculations for all four compounds and the experimental data for n3, n5, and n6. Thus, it is reasonable to propose that the differences in emission energy observed experimentally are largely a result of changes in the Au−I bond length with minor contributions from the P−Au−P bond angle distortions.

CONCLUSIONS

The results reported here show that the diphosphine ligands prefer to form bridged, binuclear complexes rather than chelated monomers. The dimers with an odd number of methylene groups in the P*n*P ligand have these methylene groups arranged in a regular zigzag fashion. However, when an even number of methylene groups is present, these groups assume a less regular, kinked arrangement. These features are

dx.doi.org/10.1021/ic301954n | *Inorg. Chem.* XXXX, XXX, XXX−XXX

seen in the related, bridged, binuclear complexes that have been observed for a number of planar, four-coordinate metal complexes formed from P*n*P-type ligands.[31−34] As the computational and experimental studies show, the tether between the phosphorus atoms imposes interesting constraints on bond distances and angles within the gold coordination sphere.

Unlike the situation with $Au_2(\mu\text{-dppe})_2Br_2$ and $Au_2(\mu\text{-dppe})_2I_2$, where the crystallization of a variety of different solvates produced significant changes in the aurophilic interactions and luminescence because of the flexibility within the molecule,[15,16] we did not encounter such variations in the complexes reported here. Only $Au^I_2(\mu\text{-P5P})_2I_2\cdot 3CHCl_3$ crystallized as a solvate. The others did not need incorporation of solvent molecules to crystallize. In none of the compounds reported here did the gold centers approach one another close enough to allow aurophilic interactions.

The four complexes reported here are luminescent as solids at room temperature. For the three trigonal planar complexes, the emission energy is more strongly correlated with changes in the Au−I bond length rather than changes in the P−Au−P angle. This observation was rationalized in terms of bonding interactions involved in these gold complexes; contraction of the Au−I bond results in a significant destabilization of the S0 surface because of an increase in the energy of the antibonding $Au(5d_{x2\text{-}y2})/I(5p_z)$ orbital. Such a large destabilization of the filled $Au(5d_{x2\text{-}y2})/I(5p_z)$ antibonding orbital is not produced upon P−Au−P bond angle distortions.

EXPERIMENTAL SECTION

Materials. A previously reported procedure was used for the preparation of (tht)AuCl (tht = tetrahydrothiophene).[35] The phosphine ligands were purchased from Alfa Inorganics.

$Au^I_2(\mu\text{-P3P})_2I_2$. A 100 mg (0.309 mmol) portion of AuI was suspended in 30 mL of dichloromethane. 1,3-Bis(diphenylphosphino)-propane (250 mg, 0.606 mmol) was added to this suspension. After stirring for 2 h, all the solids dissolved. The solution was filtered, and then the solvent was removed in a vacuum. The white solid was collected and washed with diethyl ether: yield, 160 mg (70.3%). Colorless prisms suitable for the X-ray structure determination and emission spectroscopy were obtained by slow diffusion of diethyl ether into a dichloromethane solution of the product.

Infrared spectrum: 3050w, 2923w, 1481m, 1434s, 1305w, 1097s, 1028w, 995w, 949m, 841w, 741m, 688s, 528m, 510s, 478s, 456m.

^{31}P NMR spectrum: singlet at 35.1 ppm.

$Au^I_2(\mu\text{-P4P})_2(\mu\text{-I})_2$. This complex was prepared using the method outlined for $Au_2(\mu\text{-P3P})_2I_2$ from 100 mg (0.309 mmol) of AuI and 260 mg (0.610 mmol) of 1,4-bis(diphenylphosphino)butane: yield, 190 mg (81.8%). Colorless blocks suitable for the X-ray structure determination and emission spectroscopy were obtained by slow diffusion of diethyl ether into a dichloromethane solution of the product.

Infrared spectrum: 3049w, 2922w, 1479m, 1435s, 1401w, 1099s, 1028w, 996w, 893w, 742m, 693s, 517m, 481m, 454m.

^{31}P NMR spectrum: singlet at 35.6 ppm.

$Au^I_2(\mu\text{-P5P})_2I_2\cdot 3(CHCl_3)$. This complex was prepared using the method outlined for $Au_2(\mu\text{-P3P})_2I_2$ from 265 mg (0.602 mmol) of 1,5-bis(diphenylphosphino)pentane: yield, 200 mg (84.6%). Colorless blocks suitable for the X-ray structure determination and emission spectroscopy were obtained by slow diffusion of diethyl ether into a chloroform solution of the product.

Infrared spectrum: 3049w, 2919w, 1480m,1428s, 1406w, 1102s, 1013w, 993w, 947m, 840w, 741m, 685s, 527m, 503s, 476s, 451m.

^{31}P NMR spectrum: singlet at 35.7 ppm.

$Au^I_2(\mu\text{-P6P})_2I_2$. This complex was prepared using the method outlined for $Au_2(\mu\text{-P3P})_2I_2$ from 275 mg (0.605 mmol) of 1,5-bis(diphenylphosphino)hexane: yield, 200 mg (83.2%). Colorless blocks suitable for X-ray structure determination and emission spectroscopy were obtained by slow diffusion of diethyl ether into a dichloromethane solution of the product.

Infrared spectrum: 3044w, 2913w, 1585w, 1478m,1428s, 1401w, 1102s, 1024w, 976w, 947m, 854w, 773w, 739m, 687s, 528m, 504s, 473s, 447m.

^{31}P NMR spectrum: singlet at 35.6 ppm.

X-ray Crystallography and Data Collection. The crystals were removed from the glass tubes in which they were grown together with a small amount of mother liquor and immediately coated with a hydrocarbon oil on a microscope slide. A suitable crystal of each compound was mounted on a glass fiber with silicone grease and placed in the cold stream of a Bruker SMART 1000 CCD with graphite monochromated Mo Kα radiation at 90(2) K.

The structures were solved by direct methods and refined using all data (based on F^2) using the software SHELXTL 5.1. A semiempirical method utilizing equivalents was employed to correct for absorptions. Hydrogen atoms were added geometrically and refined with a riding model.[36]

Physical Measurements. Infrared spectra were recorded on a Bruker ALPHA FT-IR spectrometer. Fluorescence excitation and emission spectra were recorded on a Perkin-Elmer LS50B luminescence spectrophotometer.

Computational Details. GOs on ground and triplet excited states were performed using Turbomole v. 6.3[37] with the crystallographic data as input structures. In addition, the singlet and triplet structures of $Au^I(PPh_2Me)_2I$ were initially calculated within Turbomole. Absorption and emission spectra were simulated using ORCA v. 2.9.0.[38] The PES was constructed for the molecule $Au^I(PPh_2Me)_2I$ using ORCA v. 2.8.20. All calculations utilized an all electron doubly polarized basis set of triple-ζ quality on all atoms except gold, which utilized a Stuttgart/Bonn pseudopotential and corresponding 19-valence electron triple-basis set. GOs were performed at the B3LYP level of theory,[39] which in ORCA made use of the RIJCOX approximation.[40] Single point energies were calculated using the B2PLY double-hybrid functional of Grimme and co-workers.[41] Absorption and emission spectra were simulated using the spectroscopically oriented configuration interaction (SORCI) approach,[42] using a CAS(4,4) reference space, a selection threshold of 1×10^{-6} E_h, a prediagonalization threshold of 10^{-4}, and a natural orbital threshold of 10^{-5}.

ASSOCIATED CONTENT

Supporting Information

X-ray crystallographic files in CIF format for $Au^I_2(\mu\text{-P3P})_2I_2$, $Au^I_2(\mu\text{-P4P})_2(\mu\text{-I})_2$, $Au^I_2(\mu\text{-P5P})_2I_2\cdot 3(CHCl_3)$, and $Au^I_2(\mu\text{-P6P})_2I_2$. This material is available free of charge via the Internet at http://pubs.acs.org.

AUTHOR INFORMATION

Corresponding Author

*E-mail: shearer@unr.edu (J.S.), albalch@ucdavis.edu (A.L.B.).

Notes

The authors declare no competing financial interest.

ACKNOWLEDGMENTS

We thank the Petroleum Research Fund (Grant 37056-AC) and the U.S. National Science Foundation (Grants CHE-1011760, CHE-0716843, and CHE-0844234) for support and Ms. K. England for experimental asistance.

REFERENCES

(1) Balch, A. L. *Struct. Bonding (Berlin)* **2007**, *123*, 1.
(2) He, X.; Yam, V. W.-W. *Coord. Chem. Rev.* **2011**, *255*, 2111.
(3) Yam, V. W. W.; Chung-Chin Cheng, E. C. C. *Chem. Soc. Rev.* **2008**, *37*, 1806.
(4) Tiekink, E. R.T.; Kang, J.-G. *Coord. Chem. Rev.* **2009**, *253*, 1627.

(5) Pyykkö, P. *Chem. Rev.* **1997**, *97*, 597.
(6) Pyykkö, P. *Angew. Chem., Int. Ed.* **2004**, *43*, 4412.
(7) Pyykkö, P. *Chem. Soc. Rev.* **2008**, *37*, 1967.
(8) Schmidbaur, H.; Schier, A. *Chem. Soc. Rev.* **2008**, *37*, 1931.
(9) White-Morris, R. L.; Olmstead, M. M.; Jiang, F.; Tinti, D. S.; Balch, A. L. *J. Am. Chem. Soc.* **2002**, *124*, 2327.
(10) White-Morris, R. L.; Olmstead, M. M.; Balch, A. L. *J. Am. Chem. Soc.* **2003**, *125*, 1033.
(11) Rios, D.; Pham, D. M.; Fettinger, J. C.; Olmstead, M. M.; Balch, A. L. *Inorg. Chem.* **2008**, *47*, 3442.
(12) Ziolo, R.; Lipton, S.; Z. Dori, Z. *Chem. Commun.* **1970**, 1124.
(13) McCleskey, T. M.; Gray, H. B. *Inorg. Chem.* **1992**, *31*, 1773.
(14) King, C.; Khan, M. N. I.; Staples, R. J.; Fackler, J. P., Jr. *Inorg. Chem.* **1992**, *31*, 3236.
(15) Lim, S. H.; Olmstead, M. M.; Balch, A. L. *J. Am. Chem. Soc.* **2011**, *133*, 10229.
(16) Lim, S. H.; Olmstead, M. M.; Balch, A. L. *Chem. Sci.* **2013**, *4*, 311−318.
(17) Barakat, K. A.; Cundari, T. R.; Omary, M. A. *J. Am. Chem. Soc.* **2003**, *125*, 14228.
(18) Sinha, P.; Wilson, A. K.; Omary, M. A. *J. Am. Chem. Soc.* **2005**, *127*, 12488.
(19) Hoshino, M.; Uekusa, H.; Ohashi, Y. *Bull. Chem. Soc. Jpn.* **2006**, *79*, 1362.
(20) Hoshino, M.; Uekusa, H.; Sonoda, S.; Takuhiro Otsuka, T.; Kaizu, Y. *Dalton Trans.* **2009**, 3085.
(21) Hoshino, M.; Uekusa, H.; Ishii, S.; Otsuka, T.; Kaizu, Y.; Ozawa, Y.; Toriumi, K. *Inorg. Chem.* **2010**, *49*, 7257.
(22) Bowmaker, G. A.; Dyason, J. C.; Healy, P. C.; Engelhardt, M.; Pakawatchai, C.; White, A. H. *J. Chem. Soc., Dalton Trans.* **1987**, 1089.
(23) (a) Weigend, F.; Ahlrichs, R. *Phys. Chem. Chem. Phys.* **2005**, *7*, 3297. (b) Schaefer, A.; Horn, H.; Ahlrichs, R. *J. Chem. Phys.* **1992**, *97*, 2571. (c) Schaefer, A.; Huber, C.; Ahlrichs, R. *J. Chem. Phys.* **1994**, *100*, 5829. (d) Eichkorn, K.; Weigend, F.; Treutler, O.; Ahlrichs, R. *Theor. Chem. Acc.* **1997**, *97*, 119. (e) Weigend, F.; Furche, F.; Ahlrichs, R. *J. Chem. Phys.* **2003**, *119*, 12753. (f) Peterson, K. A.; Figgen, D.; Goll, E.; Stoll, H.; Dolg, M. *J. Chem. Phys.* **2003**, *119*, 11113.
(24) Peterson, K. A.; Puzzarini, C. *Theor. Chem. Acc.* **2005**, *114*, 283.
(25) Figgen, D.; Rauhut, G.; Dolg, M.; Stoll, H. *Chem. Phys.* **2005**, *311*, 227.
(26) Neese, F. *Coord. Chem. Rev.* **2009**, *253*, 526.
(27) Neese, F. *J. Chem. Phys.* **2003**, *119*, 9428.
(28) Neese, F.; Petrenko, T.; Ganyushin, D.; Olbrich, G. *Coord. Chem. Rev.* **2007**, *251*, 288.
(29) Schwabe, T.; Grimme, S. *Acc. Chem. Res.* **2008**, *41*, 569.
(30) Neese, F.; Hansen, A.; Wennohs, F.; Grimme, S. *Acc. Chem. Res.* **2009**, *42*, 641.
(31) Balch, A. L.; Tulyathan., B. *Inorg.Chem.* **1977**, *16*, 2840.
(32) Wang, H.-H.; Pignolet, L. H.; Reedy, P. E., Jr.; Olmstead, M. M.; Balch, A. L. *Inorg. Chem.* **1987**, *26*, 377.
(33) Balch, A. L.; Davis, B. J.; Olmstead, M. M. *Inorg. Chem.* **1990**, *29*, 3066.
(34) Samar, D.; Fortin, J.-F.; Fortin, D.; Decken, A.; Harvey, P. D. *J. Inorg. Organomet. Polym* **2006**, *15*, 411.
(35) Uson, R.; Laguna, A.; Laguna, M. *Inorg. Synth* **1989**, *26*, 85.
(36) Sheldrick, G. M. *Acta Crystallogr., Sect. A* **2008**, *64*, 112.
(37) *Turbomole*, version 6.2; University of Karlsruhe and Forschungszentrum Karlsruhe GmbH: Karlsruhe, Germany, 2011.
(38) (a) Neese, F. *ORCA, An ab Initio, Density Functional, and Semiempirical Program Package*, version 2.8.20; Institute for Physical and Theoretical Chemistry, Universität Bonn: Bonn, Germany, 2010. (b) Neese, F. *ORCA, An ab Initio, Density Functional, and Semiempirical Program Package*, version 2.9; Max-Planck-Institute for Bioninorganic Chemistry: Mülheim a. d. Ruhr, Germany, 2011.
(39) (a) Vosko, S. J.; Wilk, M.; Nusair, M. *Can. J. Phys.* **1980**, *58*, 1200. (b) Becke, A. *J. Chem. Phys.* **1986**, *84*, 4524. (c) Becke, A. *J. Chem. Phys.* **1988**, *88*, 1053. (d) Becke, A. *Phys. Rev. A* **1988**, *38*, 3098. (e) Perdew, J. P. *Phys. Rev. B* **1986**, *34*, 7406. (f) Perdew, J. P. *Phys. Rev. B* **1986**, *33*, 8822.
(40) Neese, F.; Wennmohs, F.; Hansen, A.; Becker, U. *Chem. Phys.* **2009**, *356*, 98.
(41) Schwabe, T.; Grimme, S. *Acc. Chem. Res.* **2008**, *41*, 569.
(42) Neese, F. *J. Chem. Phys.* **2003**, *119*, 9428.